Scientific Justification

One of the fundamental questions about supermassive black holes (SMBHs) is why some are active while others, located in apparently similar galaxies, are not. Since almost all massive galaxies host nuclear SMBHs (Magorrian 1998), it is clear that a trigger is required to "turn on" the SMBH. However, the trigger mechanism remains elusive. We believe this is because — until now — an unbiased survey has been impossible, since AGN emission in the IR, optical, UV, and soft X-ray is obscured in a large fraction ($\sim$50%) of AGN by dust and gas in the line of sight (e.g. Mushotzky 2004) and only a small fraction can be radio selected. Further, other indicators of activity in obscured objects, such as IR continuum and [OIII] (Heckman et al 2005) are *indirect* measures of AGN power, and can be strongly affected by star formation and extinction. Alone among all tracers, hard X-ray emission ($E >$ 20keV) is (1) not strongly affected by obscuration (τ due to photoelectric absorption is small) and (2) directly associated with the AGN.

Until recently, a high-sensitivity hard X-ray survey was impossible due to insufficient angular resolution to identify 'unique' counterparts in other wavebands and insufficient solid angle and sensitivity to yield a large sample. This situation has been radically changed by the Swift BAT survey (Markwardt et al 2005, Tueller et al 2008, 2010), which has detected $\sim$850 AGN above a threshold of 5.5σ. The BAT data are $\sim$30 times more sensitive than previous all-sky surveys (Levine et al. 1984). Indeed, BAT has revealed a significant fraction of AGN that would not have been identified in previous surveys at *any* waveband.

We have found (e.g. Koss et al 2011ab, 2012) that the properties of host galaxies of the BAT-selected AGN are quite different from matched sets of non-AGN hosts or SDSS-selected AGN hosts. At high stellar masses, the BAT AGN are $\approx$100X more likely to be in spiral morphologies than inactive galaxies (Koss et al. 2011a). This difference indirectly suggests that a subset of AGN activity may be driven by stochastic accretion of cold gas that should be more prominent among these late-type systems (Hopkins & Hernquist 2006). Recent theoretical work (e.g. Hopkins et al 2005) shows strong connections between the obscuring material and the growth of the black hole. It seems that growth requires large densities of gas in the centers of galaxies which naturally generate obscuring column densities, and thus should be ideally studied via molecular line imaging possible for low redshift objects. Contrary to work based on prior (i.e. biased) surveys, the CO detection rate of BAT-selected AGN is over an order of magnitude greater than for a comparison sample of SDSS AGN chosen to have the same mass and redshift, and we find a correlation between CO and hard X-ray luminosity. This suggests that we may have found the long-sought link between fuel supply and AGN triggering.

We believe that these results were not found in previous CO surveys of AGN due to selection biases. For example, the best existing high-resolution study, NUGA, includes among its selection criteria the availability of high-resolution optical/NIR HST data, thus biasing against obscured AGN; further, NUGA picked objects known to be ideal for high-resolution CO detection and thus these objects are unrepresentative and under-represent high X-ray luminosity AGN. By contrast, our sample uses the first unbiased AGN survey and thus provides a fundamentally new sample for investigating the origin of AGN activity.

Our team has obtained a wide range of complementary data, including Spitzer IR spectra (Weaver et al 2011), optical spectra and imaging (Winter et al 2011; Koss et al 2011a), X-ray spectra (Winter et al 2009) and Herschel FIR data (Fig 1, top). However, our CO results used the JCMT, yielding 2 kpc resolution at best, inadequate even to separate out the galaxy disk. We have CARMA observations of CO(1-0) scheduled for 10 BAT AGN at $2''$ resolution to map low excitation gas. However, CO(3-2) is needed to probe gas affected by AGN radiation, since the higher J lines are known to be enhanced near AGN (Matsushita et al 2004, Krips et al 2011). CO(2-1) and (1-0) are unreliable tracers of this gas because they are more easily excited and only trace cloud surfaces (Hsieh et al 2011, Krips et al 2011). The ratio of CO(3-2) to CO(1-0) flux is known to be a good indicator of molecular gas excited by an AGN (Mao et al 2010). Indeed, the SMA has already successfully observed CO(3-2) in the prototypical AGN NGC1068 (Krips et al 2011; Tsai et al 2012), where the CO (3-2)((2-1) and (3-2)/(1-0) line ratios were found to be substantially enhanced relative to galactic disks, with the (3-2) line 4x times stronger than the (2-1) line and 18x stronger than the (1-0) line, demonstrating the importance of observing the (3-2) CO line rather than the (2-1) line so as to probe the gas affected by the AGN. A further advantage of observing (3-2) CO over (2-1) is that we can simultaneously obtain HCN and HCO^+, known to be superb AGN tracers.

We propose SMA CO(3-2) observations of four BAT AGN, selected so that we can investigate the poorly probed high X-ray luminosity regime. We select the four BAT AGN observable in the Spring that are close enough that the $0.8''$ resolution of the SMA extended array is sufficient to probe the X-ray dominated (XDR) region surrounding the AGN, where the chemistry and excitation is expected to be significantly influenced by the AGN. Using the results of Spinoglio et al (2012), for the luminosities of our target AGN we expect the XDR to extend over a diameter of 200 to 500 pc. Three of our targets (NGC 4388, NGC 3516, NGC 5506) are near enough that they can be studied at a scale of ~100-150pc with a $0.8''$ beam. The fourth object (NGC 5995) is further away and thus will have a coarser resolution (~400pc), but it is the most luminous and thus should have a correspondingly larger XDR size. These four galaxies enable us to cover a range of Seyfert types (1h, 1i, 1.5, 2).

Science goals: We seek to understand why the hard X-ray selected AGN are systematically more luminous in CO, why CO and hard X-ray luminosity are correlated, and whether this implies we have found links between fuel supply, AGN triggering, and AGN effects on star formation. Specifically, we hope to test whether XDRs can explain the CO-hard X-ray correlation in AGN. Using SMA CO(3-2) data in combination with CO(1-0) data from CARMA, we can estimate the density and temperature of the gas with LVG analysis (Goldreich & Kwan 1974) to gain insight into its heating mechanisms and the effect of the XDR. We will determine the ratio of CO(3-2) to CO(1-0) intensities, R_{31}, which quantifies the molecular gas excitation and is correlated with the star formation rate surface density to disentangle the gas nearby and directly affected by the AGN from the star-forming gas further out. We can thus determine the relative fractions of molecular gas associated with AGN activity or star formation, which indicates the source of fuel for the AGN. We will relate the CO distribution and velocity field to other properties of the AGN such the gas column densities implied by the AGN X-ray spectra. With high-angular resolution kinematic data, we will also look for evidence of AGN fueling and molecular winds/feedback.

Technical Justification

As described in the Science Justification, we need subarcsecond resolution in the (3-2) CO line to probe XDRs in high X-ray luminosity AGN, indicating the need for the SMA Extended Array at 345 GHz. In single Rx 4GHz mode with 128 channels per chunk, we can average the 0.7 km/sec channel resolution to 30 km/sec to maximize signal-to-noise while preserving the kinematic information. The 4 GHz band spans 3500 km/s, easily sufficient for gas orbiting the AGN and useful for searching for winds. HCN and HCO^+(4-3) can be observed in the upper sideband. Using the SMA sensitivity calculator, we expect rms ~20 mJy/bm in a 30 km/s channel at 6 hours per source in typical weather at the CO frequency corresponding to our typical z. We have detected CO (3-2) in all four targets at the JCMT (Fig 2) with a $14''$ beam. Herschel images trace FIR emission likely to be correlated with CO emission; these images (Fig 3) show unresolved (<s5″) cores that contain most of the FIR emission within the $14''$ JCMT beam; even for NGC 4388, for which Herschel also shows extended flux, more than 70% of the emission is unresolved. Assuming then that in the worst case in each channel the CO(3-2) flux observed at the JCMT is uniformly distributed over $5''$, we expect flux $> 1 - 3\sigma$ in each channel over most of the line profile.

References: • Heckman, T., et al. 2005, ApJ, 634, 161 • Hopkins, P. F., et al. 2005, ApJ, 630, 705 • Hopkins, P. F., & Hernquist, L. 2006, ApJS, 166, 1 • Hsieh, P., et al. 2011, ApJ, 736, 129 • Koss, M., et al. 2012, ApJL, 746, 22 • Koss, M., et al. 2011a, ApJ, 739, 57 • Koss, M., et al. 2011b, ApJL, 735, 42 • Krips, M., et al. 2011, ApJ, 736, 37 • Levine, A. M., et al. 1984, ApJS, 54, 581 • Magorrian, J., et al. 1998, ApJ, 115, 2285 • Mao, R., et al. 2010, ApJ, 724, 1336 • Markwardt, C. B., et al. 2005, ApJ, 633, 77 • Matsushita, S., et al. 2004, ApJL, 616, 55 • Mushotzky, R. 2004, in Supermassive Black Holes in the Distant Universe, Vol. 308, ed. A. J. Barger (Dordrecht: Kluwer), 53 • Spinoglio L., et al. 2012, arXiv:1208.6132 [astro-ph.GA] • Tsai, M., et al. 2012, ApJ, 746, 129 • Tueller, J., et al. 2008, ApJ, 681, 113 • Tueller, J., et al. 2010, ApJS, 186, 378 • Weaver, K. A., et al. 2010, ApJ, 716, 1151 • Winter, L. M., et al. 2010, ApJ, 710, 503 • Winter, L. M., Mushotzky, R. F., Reynolds, C. S., & Tueller, J. 2009, ApJ, 690

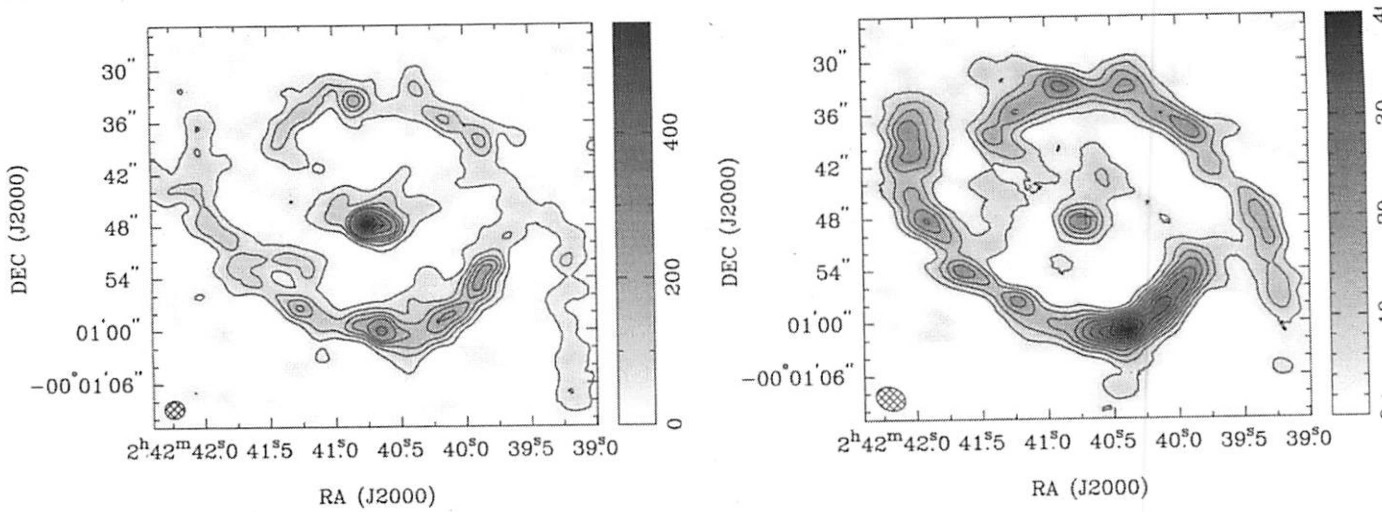

Fig. 1.— Integrated intensity maps (in units of Jy beam^{-1} km s^{-1}) of NGC 1068 taken with the SMA from Tsai et al 2012. (*Left*) CO(3-2) integrated intensity. Contour levels are at 10, 20, 30, 40, 50, 60, 70, 80, 90, 100, 110, and 130 σ, where $1\sigma = 4.0$ Jy beam^{-1} km s^{-1}. The synthesized beam is $2.29'' \times 2.00''$($\sim 160 \times 140$ pc^2). (*Right*) CO(1-0) integrated intensity. Contour levels are at multiples of 5σ, where $1\sigma = 0.81$ Jy beam^{-1} km s^{-1}. The synthesized beam is $3.46'' \times 2.56''$.

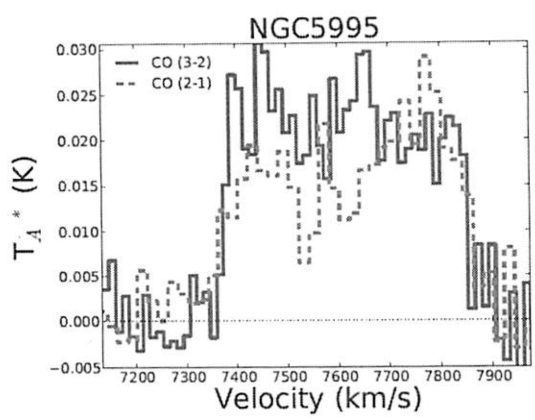

Fig. 2.— CO spectra of NGC 5995, 3-2 (blue) and 2-1 (red).

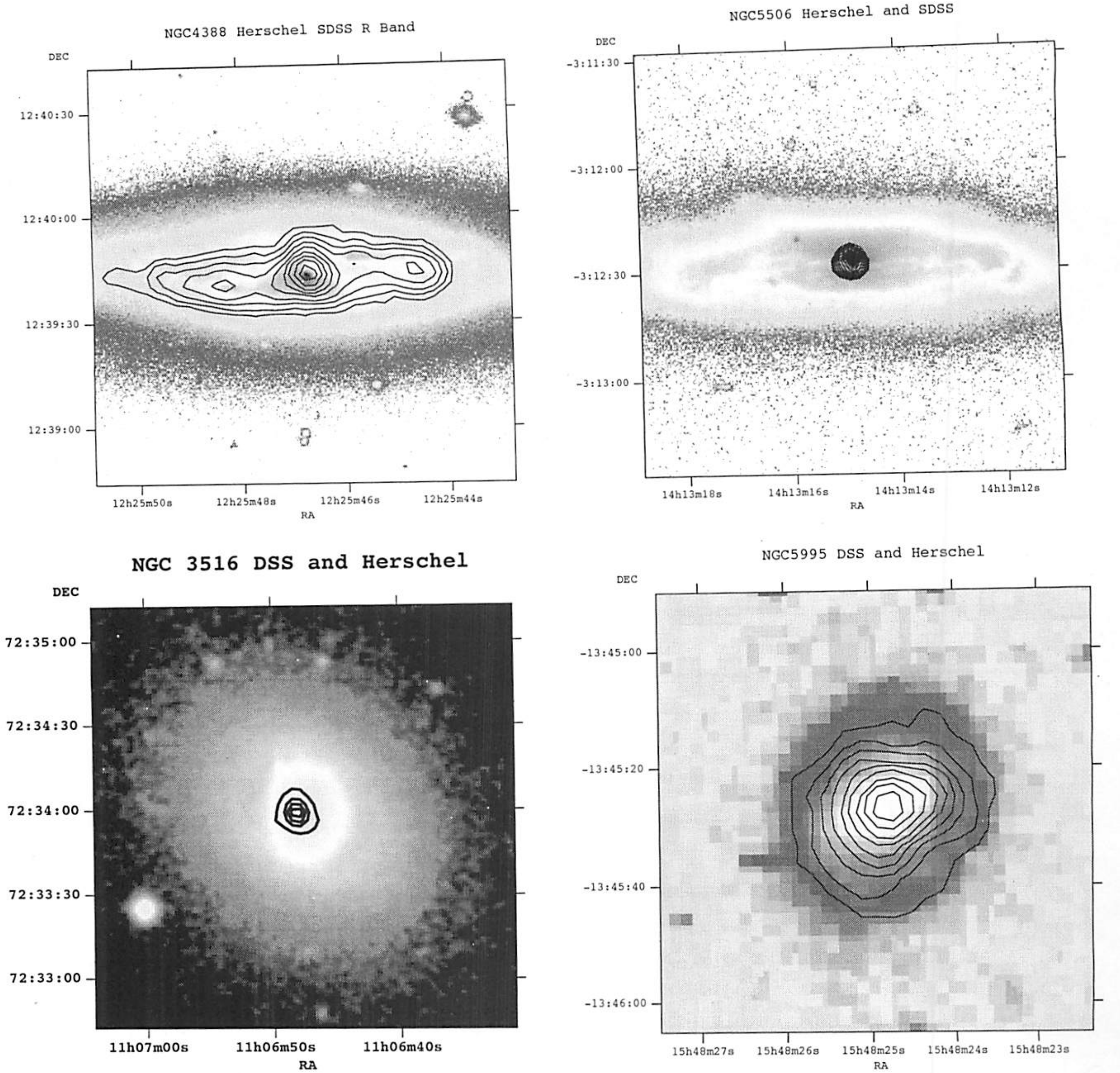

Fig. 3.— Top: SDSS (color- log stretch) and Herschel (contours logarithmically spaced) images of NGC4388 (*top left*) and NGC5506 (*top right*) NGC 3516 (*bottom left*), NGC 5995 (*bottom right*).

ASTR670
Spring 2011
Prof. Alberto Bolatto

Homework 1

1) Use the discussion by Carl Heiles (1979) to estimate the energy necessary to blow a bubble of 100 pc radius in the local ISM. What about a 1 kpc radius bubble?

2) Let us try to estimate the amount of energy necessary to blow out a chimney in the cold ISM of the galaxy at about the Solar circle. This is, by necessity, a very back-of-the-envelope, wave-of-the-hands, fly-by-the-seat-of-your-pants calculation. You get the idea.

Use the simplified vertical potential for the Galactic disk in Eq. 40 of Kuijken & Gilmore (1989) paper I. Look up the values of the parameters in the follow up paper (same authors, same year, paper II). To avoid being confused by the strange units please convert everything to cgs. Assume the density of the cold ISM is $n \sim 1$ cm^{-3} on the plane, with an exponential vertical scale height $H \sim 250$ pc.

Estimate how much energy do you need to blow a 100 pc radius tunnel in this material, sending it to 1kpc height over the Galactic disk.

3) Use the ratio of the thermal energy density over the emissivity discussed in class to find out the cooling time through radiative processes of a $T \sim 10^6$ K plasma with density $n \sim 0.001$ cm^{-3}. What is the cooling time for a $T \sim 10^7$ K plasma?

HII Regions (Osterbrock §2)

Ionization balance:

$$n(H^0)\int_{\nu_0}^{\infty} \underbrace{\frac{4\pi J_\nu}{h\nu}}_{\phi_\nu} \underbrace{a_\nu(H^0)}_{\text{ionization cross-section } (\sigma^{bf} \text{ for Spitzer})} d\nu = n(H^0)\cdot\Gamma(H^0) = n_e n_p\, \underbrace{\alpha(H^0,T)}_{\text{recomb. coeff. } [cm^{+3}\, s^{-1}]}$$

$J_\nu \rightarrow$ mean intensity $\left[\frac{erg}{cm^2}\right]$

$\Rightarrow$ # of photons per unit area $\triangleq \phi_\nu$

$$4\pi J_\nu = \frac{\overset{\text{star radius}}{R^2}}{r^2}\,\underbrace{\pi F_\nu(0)}_{\text{flux at star surface}} = \frac{L_\nu}{4\pi r^2} \quad [erg\ cm^{-2}\, s^{-1}\, Hz^{-1}]$$

$$\Rightarrow n(H^0)\int \frac{L_\nu}{4\pi r^2}\frac{1}{h\nu}\cdot a_\nu\, d\nu = n_e n_p \alpha$$

$$\Rightarrow \frac{n(H^0)}{4\pi r^2}\int \frac{L_\nu}{h\nu} a_\nu d\nu = n_e n_p \alpha$$

$n^2(1-x)^2$

$x \cdot n$

$x = 0.5 \Rightarrow$

$$\frac{1}{4\pi r^2}\int \frac{L_\nu}{h\nu} a_\nu d\nu = \frac{n}{2}\alpha$$

$$\Rightarrow \frac{1}{2\pi\alpha n}\int \frac{L_\nu}{h\nu} a_\nu d\nu = r^2$$

<u>Ex</u>: 5pc away from O7.5 star

$T_* = 39{,}700\ K$

$$Q(H^0) = \int_{\nu_0}^{\infty} \frac{L_\nu}{h\nu} d\nu \approx 1\times10^{49}\ s^{-1}$$

$$a_\nu(H^0) \approx 6\times10^{-18}\ cm^{-2}$$

$$\Gamma(H^0) = \frac{1}{4\pi r^2}\cdot Q(H^0)\cdot a_\nu(H^0) \approx 1\times10^{-8}\, s^{-1} \triangleq \underbrace{\tau_{ph}^{-1}}_{\text{lifetime of atom before ionization}}$$

$$\alpha(H^0,T) \approx 4\times10^{-13}\ cm^3\, s^{-1}$$

$$\Rightarrow n(H^0)\cdot\Gamma(H^0) = n_e n_p \alpha(H^0,T) = n^2(H^0)\cdot(1-\xi)^2 \qquad \xi \triangleq \text{neutral fraction}$$

$$n(H^0) = \xi\, n(H)$$

$$\Rightarrow \xi\, \cancel{n(H)}\cdot\Gamma(H^0) = (1-\xi)^2\cdot n^{\cancel{2}}(H)\cdot\alpha(H^0,T)$$

$$\frac{\xi}{(1-\xi)^2} = \frac{n(H)}{\Gamma(H^0)}\,\alpha(H^0,T) \qquad \text{assume } n(H) = 10\ cm^{-3}$$

$$\xi = \frac{10\ cm^{-3}}{1\times10^{-8}\ s^{-1}}\cdot 4\times10^{-13}\ cm\ s^{-1} = 4\times10^{-4} \Rightarrow \boxed{\text{H is completely ionized}}$$

Thickness of region over which ionization state changes is $l \sim (n(H^0) \cdot a_\nu)^{-1}$ cm ; mean free path of ionizing photon $\Rightarrow$ $l \sim \frac{1}{n(H^0) \cdot a_\nu} \sim 0.1$ pc in our example

Permitted transitions for H have $A(nL \to n'L') \sim 10^4 - 10^8\ s^{-1}$

$\Rightarrow$ The lifetimes of the excited levels are $\tau_{nL} = \frac{1}{\sum\limits_{n'<n} \sum\limits_{L'=L\pm1} A_{nL,n'L'}} \sim 10^{-4} - 10^{-8}$ s

The 2^2S has no allowed transitions to 1^2S because $L' = L \pm 1$ is not possible, but the 2-photon transition has a probability $A(2^2S \to 1^2S) = 8.23\ s^{-1}$ $\Rightarrow$ the lifetime is 0.12^s

$\boxed{\text{Nebular approx.}}$

These are all much shorter than our previous estimate of the lifetime before ionization ($\tau_{pn} \approx 10^8$ s) $\Rightarrow$ All neutral H is in the ground state in $\underline{HII}$ regions!

$\Rightarrow$ We only care about a_ν for the 1^2S level.

$$a_\nu(Z) = \frac{A_0}{Z^2} \left(\frac{\nu_1}{\nu}\right)^4 \cdot \frac{\exp\left(4 - (4 \tan^{-1}\varepsilon / \varepsilon)\right)}{1 - \exp(-2\pi/\varepsilon)} \ \text{cm}^2 \quad \text{for } \nu \geq \nu_1 .$$

$\boxed{\text{photoionization cross-section}}$

$$A_0 = \frac{2^9 \pi}{3 e^4} \left(\frac{1}{137.0}\right) \pi a_0^2 = 6.30 \times 10^{-18} \ \text{cm}^2$$

$$\varepsilon = \sqrt{\frac{\nu}{\nu_1} - 1} \quad , \quad h\nu_1 = Z^2 h\nu_0 = 13.6 Z^2 \ \text{eV}$$

$a_\nu \sim \nu^{-3}$ close to the threshold ν_1

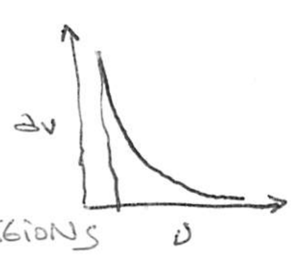

$\Rightarrow$ harder photons penetrate further into the material

2.2 Photoionization and Recombination of Hydrogen

Figure 2.1 is an energy-level diagram of H; the levels are marked with their quantum numbers n (principal quantum number) and L (angular momentum quantum number), and with S, P, D, F, . . . standing for $L = 0, 1, 2, 3, \ldots$ in the conventional notation. Permitted transitions (which, for one-electron systems, must satisfy the selection rule $\Delta L = \pm 1$) are marked by solid lines in the figure. The transition probabilities $A(nL, n'L')$ of these lines are of order 10^4 to 10^8 s^{-1}, and the corresponding mean lifetimes of the excited levels,

$$\tau_{nL} = \frac{1}{\sum\limits_{n'<n} \sum\limits_{L'=L\pm 1} A_{nL,n'L'}}, \tag{2.3}$$

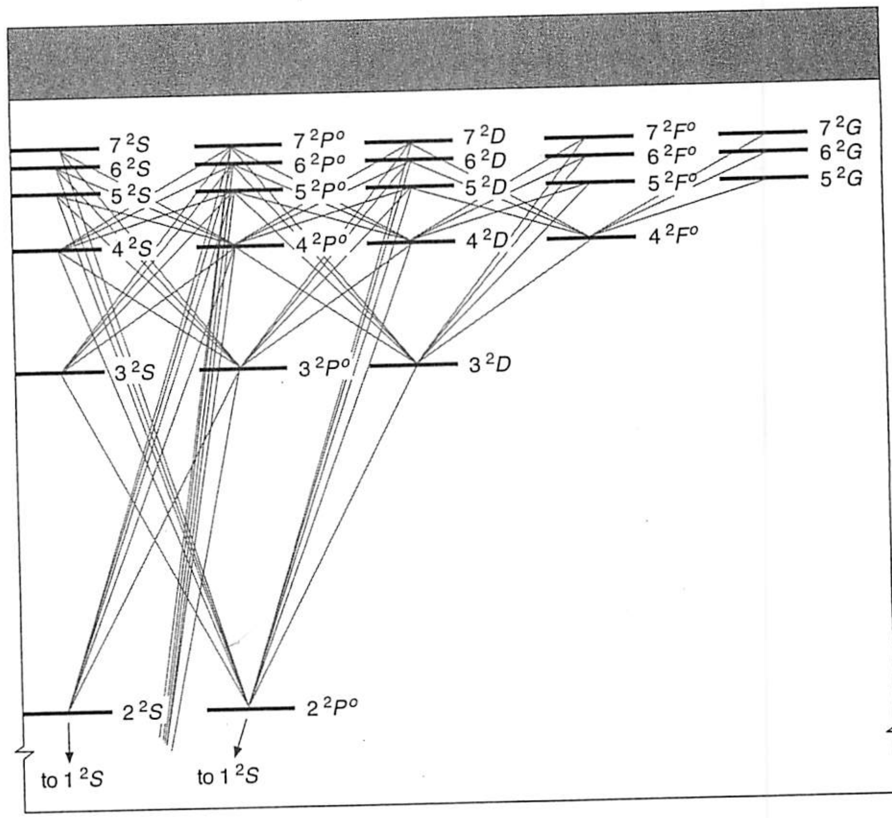

Figure 2.1
Partial energy-level diagram of H I, limited to $n \leq 7$ and $L \leq G$. Permitted radiative transitions to levels $n < 4$ are indicated by solid lines.

OOSTERBROCK

what about recombination?

cross-section to collisions among electrons is large (charged particles) $\Rightarrow$ es are thermalized very quickly after ionization

$$\alpha_{n^2L}(H^\circ, T) = \int_0^\infty u \, \sigma_{n^2L}(H^\circ, u) \, f(u) \, du$$ recombination coeff to level n^2L

$$f(u) = \frac{4}{\sqrt{\pi}} \left(\frac{m}{2kT}\right)^{3/2} u^2 \exp(-mu^2/kT)$$ Maxwell-Boltzmann

$$\sigma(H^\circ, u) \sim u^{-2} \Rightarrow u \cdot \sigma \sim u^{-1} \sim T^{-1/2}$$

Effective recombination coefficient is summed over all levels. in the <u>nebular approximation</u>:

$$\alpha_A = \sum_{n,L} \alpha_{n^2L}(H^\circ, T) = \sum_n \sum_{L=0}^{n-1} \alpha_{nL}(H^\circ, T) = \sum_n \alpha_n(H^\circ, T)$$

$n^2L \longrightarrow 1^2S$
capture at final level

$\cancel{\sigma^{fb}_n(\nu) = \frac{2 h^2 \nu^2}{m_e^2 c^2 u^2} \sigma^{bf}_n(\nu)}$ ~~Milne relation~~

$\alpha_A \rightarrow$ recombination to ground level (effective)
$\alpha_B \rightarrow$ " " 2^2S (effective)

	5000 K	10000 K	20000 K
α_A	6.82×10^{-13}	4.18×10^{-13}	2.51×10^{-13}
α_B	4.54×10^{-13}	2.59×10^{-13}	1.43×10^{-13}

Photoionization:

$$n(H^0)\int_{\nu_0}^{\infty}\frac{4\pi J_\nu}{h\nu}a_\nu\,d\nu = n_p n_e \alpha_A(H^0,T)$$

For radiation with $\nu > \nu_0$, (ν_0 corresponds to 13.6 eV)

$$\frac{dI_\nu}{ds} = \underbrace{-n(H^0)a_\nu}_{K_\nu} I_\nu + j_\nu$$

We can break up I_ν into a stellar and a diffuse component

$$I_\nu = I_{\nu s} + I_{\nu d}$$

The diffuse component comes from recombinations directly to the ground state ($n=1$)

$$\underbrace{E_\gamma}_{\text{photon}} = \underbrace{E_e}_{\text{electron}} + \underbrace{E_n}_{\text{level}} > 13.6 \text{ eV}$$

$E_e \sim 1$ eV

$E_2 \sim \frac{1}{4} E_1 \sim 3.4$ eV

⇒ only photons that come from ground state recombinations can ionize the nebula

$$E_\gamma = E_e + E_1 \sim 1 + 13.6 \text{ eV} \gtrsim E_1$$

Going back to radiation: Stellar part

$$4\pi J_{\nu s} = \pi F_{\nu_s}(r) = \pi F_{\nu_s}(\underset{\substack{\uparrow \\ \text{stellar radius}}}{R}) \cdot \frac{R^2 e^{-\tau_\nu(r)}}{r^2}$$

$$\tau_\nu(r) = \int_0^r n(H^0, r')\, a_\nu \cdot dr'$$

$$\tau_\nu(r) = \frac{a_\nu}{a_{\nu_0}} \cdot \tau_0(r)$$
optical depth at ionization threshold

For the diffuse part:

$$\frac{dI_{\nu d}}{ds} = -n(H^0)\, a_\nu I_{\nu d} + j_\nu$$

For $kT \ll h\nu_0$ the only source of ionizing radiation is the recapture of e to the ground 1^2s level, as we just saw:

$$j_\nu(T) = \frac{2h\nu^3}{c^2}\left(\frac{h^2}{2\pi m k T}\right)^{3/2} a_\nu \cdot \exp\left(-\frac{h(\nu-\nu_0)}{kT}\right) n_p n_e$$
(strongly peaked @ ν_0)

Number of photons generated by recombination:

$$4\pi \int_{\nu_0}^{\infty} \frac{j_\nu}{h\nu}\, d\nu = n_p n_e\, \alpha_1(H^0, T)$$
(i.e., it's the number of recombinations to the ground level)

Since $\alpha_1 = \alpha_{1S} < \alpha_A$, $J_{\nu d} < J_{\nu s}$.

For an optically thin nebula, $J_{\nu d} \approx 0$. It can be calculated iteratively.

For an optically thick nebula: "on the spot" approximation

no ionizing photons can escape, so every diffuse photon is absorbed somewhere

$$4\pi \int \frac{j_\nu}{h\nu}\, dV = 4\pi \int n(H^0) \frac{a_\nu J_{\nu d}}{h\nu}\, dV$$

The approximation assumes this holds locally, so

$$J_{\nu d} = \frac{j_\nu}{n(H^0) \cdot a_\nu}$$ "on the spot"

(essentially correct because diffuse photons have $\nu \sim \nu_0 \Longrightarrow a_\nu$ is big)

So, going back to the ionization – recomb. equilibrium equation:

$$n(H^\circ)\cdot\int_{\nu_0}^{\infty}\frac{4\pi J_\nu}{h\nu}a_\nu d\nu = n_p n_e \alpha_A(H^\circ,T)$$

$$J_\nu = J_{\nu s} + J_{\nu d}$$

$$J_{\nu s} = \frac{F_{\nu s}}{4}(R)\cdot\frac{R^2 e^{-\tau_\nu}}{r^2}$$

$$J_{\nu d} = \frac{h\nu}{4\pi}\cdot\frac{n_p n_e \alpha_1(H^\circ,T)}{n(H^\circ)\,a_\nu}$$ ← comes from $4\pi\int\frac{j_\nu}{h\nu}d\nu = n_p n_e\alpha_1$

$$\Rightarrow\quad n(H^\circ)\cdot\frac{R^2}{r^2}\int_{\nu_0}^{\infty}\frac{\pi F_{\nu s}(R)}{h\nu}a_\nu e^{-\tau_\nu}d\nu + n_p n_e\alpha_1(H^\circ,T) = n_p n_e\alpha_A(H^\circ,T)$$

$$\Rightarrow\quad n(H^\circ)\frac{R^2}{r^2}\int_{\nu_0}^{\infty}\frac{\pi F_{\nu s}(R)}{h\nu}a_\nu e^{-\tau_\nu}d\nu = n_p n_e(\alpha_A-\alpha_1) = n_p n_e\alpha_B(H^\circ,T)$$

$$\alpha_B(H^\circ,T) = \sum_{2}^{\infty}\alpha_n(H^\circ,T)$$

↑ comes from stellar atmosphere calculations

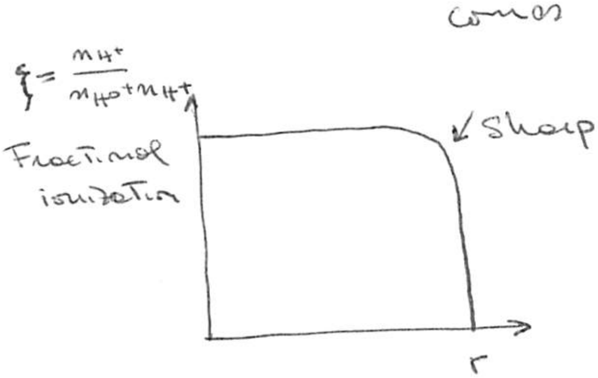

$$\frac{d\tau_\nu}{dr} = n(H^\circ)\cdot a_\nu \quad\Rightarrow\quad \frac{R^2}{r^2}\int_{\nu_0}^{\infty}\frac{\pi F_{\nu_s}(R)}{h\nu}\cdot\frac{d\tau}{dr}\cdot e^{-\tau}\cdot d\nu = n_p n_e\alpha_B(H^\circ,T)$$

$$\Rightarrow\quad R^2\int_{\nu_0}^{\infty}\frac{\pi F_{\nu_s}(R)}{h\nu}d\nu\,\underbrace{\int_0^{\infty}e^{-\tau}d\tau}_{1} = \int_0^{\infty}n_p n_e\alpha_B\, r^2\,dr$$

Since $n_p = n_e \approx n(H)$ inside r_1 and $n_p = n_e = 0$ outside

$$\Rightarrow \quad R^2 \int_{\nu_0}^{\infty} \frac{\pi F_\nu(R)}{h\nu}\, d\nu = \int_0^{r_1} n_p n_e \, \alpha_B \, r^2 \, dr$$

$$4\pi R^2 \int_{\nu_0}^{\infty} \frac{\pi F_\nu}{h\nu}\, d\nu = \int_{\nu_0}^{\infty} \frac{L_\nu}{h\nu}\, d\nu = Q(H^0) = \frac{4\pi}{3} r_1^3 \cdot n_H^2 \cdot \alpha_B(H^0, T)$$

(N_u for Spitzer) (Draine eq. 15.1)

$\Rightarrow$ Total number of ionizing photons balances Total number of recombinations to excited levels inside r_1.

"Strömgren Sphere", 1939

Type	T_* (K)	$\log Q(H^0)$ (ph/s)	r_1 (pc) for $n = 1\ cm^{-3}$
O3 V	51200	49.87	122
O7.5V	39700	49.00	63
B0V	33300	48.16	33

(see Draine Table 15.1)

$$EM = \frac{4}{3} n_H^2 r_1 \approx 4.22 \times 10^4 \; Q_{49}(H^0)^{1/3} \; n_2^{4/3} \; T_4^{0.28} \; cm^{-6}\, pc$$

averaged over πr_1^2 Ω solid angle

$$r_1 = 9.77 \times 10^{18} \; Q_{48}^{1/3}(H^0) \; n_2^{-2/3} \; T_4^{0.28} \; cm$$

$$\text{mean free path} = \frac{1}{n(H^0)\,\sigma}$$

Table 5.1 gives the number $S(0)$ of photons in the Lyman continuum of hydrogen and $S(1)$ in the Lyman continuum of helium (see later) emitted by different types of hot stars, calculated from stellar atmosphere models by Schaerer & de Koter [456]. We can readily derive U from this table. For hydrogen, the results of these models are not much different from those of Panagia [395] which are widely used, but they are very different for helium.

Table 5.1. Fluxes of ionizing photons $S_0 = N_{LyC}(\text{H I})$ and $S_1 = N_{LyC}(\text{He I})$ in the hydrogen and helium Lyman continua for various types of hot stars with solar abundances, from Schaerer & de Koter [456].

Sp. type	V(dwarf)			III(giant)			I(supergiant)		
	$\log T_{eff}$ K	$\log S_0$ s^{-1}	$\log S_1$ s^{-1}	$\log T_{eff}$ K	$\log S_0$ s^{-1}	$\log S_1$ s^{-1}	$\log T_{eff}$ K	$\log S_0$ s^{-1}	$\log S_1$ s^{-1}
O3	4.710	49.85	49.42	4.707	49.97	49.52	4.705	50.09	49.63
O4	4.687	49.68	49.23	4.683	49.84	49.38	4.678	50.02	49.56
O4.5	4.676	49.58	49.12	4.670	49.78	49.32	4.665	49.98	49.53
O5	4.664	49.48	49.01	4.657	49.71	49.25	4.650	49.94	49.47
O5.5	4.652	49.38	48.86	4.644	49.64	49.16	4.636	49.88	49.35
O6	4.639	49.28	48.75	4.630	49.56	49.05	4.620	49.81	49.24
O6.5	4.626	49.17	48.62	4.615	49.47	48.91	4.604	49.73	49.12
O7	4.613	49.05	48.44	4.601	49.36	48.75	4.588	49.64	48.91
O7.5	4.599	48.93	48.25	4.585	49.24	48.53	4.571	49.53	48.65
O8	4.585	48.80	48.05	4.569	40.09	48.14	4.553	49.42	48.37
O8.5	4.570	48.64	47.74	4.553	48.94	47.80	4.534	49.29	48.05
O9	4.555	48.46	47.37	4.536	48.76	47.40	4.515	49.12	47.67
O9.5	4.539	48.25	46.92	4.518	48.56	46.95	4.495	48.90	47.21
B0	4.523	48.02	46.41	4.499	48.33	46.47	–	–	–
B0.5	4.506	47.77	45.86	4.479	48.11	46.03	–	–	–

Photons with energy only slightly higher than 13.6 eV are mostly absorbed by hydrogen. Those with higher energies can be absorbed by helium, nitrogen, etc. In practice, the most efficient element at a given photon energy is the one which has an ionization threshold immediately smaller than this energy. This results from the fast variation in ν^{-3} of the photoionization cross-sections. A consequence of this is the formation of an ionization structure in relatively uniform gaseous nebulae.

Photons with an energy larger than 24.6 eV, the ionization potential of helium, produce a region of ionized helium in the inner zone of the H II region. Table 5.1 gives the number of helium-ionizing photons as a function of the spectral type of the central star. If this star is hot enough, the He II zone is co-extensive with the H II one. This occurs when $S_1/S_0 > 0.1$, i.e. for stars hotter than O8. He III (54.4 eV) is only visible around the very hottest stars (some Wolf–Rayet stars). Oxygen having an ionization potential very close to that of hydrogen, the O II zone is co-extensive with the H II zone. O III (35.1 eV) is only found in the central regions if the star is very hot.

LEQUEUX

Relation between recombination and photoionization rates: Milne equation (Spitzer 5-3)
Draine 3.31

(a) # of recombinations per unit volume

$$n_+ \cdot n_e \, \sigma_{fb} \cdot f(u)\, u\, du$$

(b) # of photoionization per unit time in a BB rad. field

$$\frac{4\pi}{h\nu} n_0 \sigma_{bf} \cdot \underbrace{\left(1 - e^{-h\nu/kT}\right)}_{\uparrow} B_\nu \, d\nu$$

net photoionization after subtraction "stimulated recombinations"

In thermodyn. eq.:

$$\text{(a)} = \text{(b)} \Rightarrow \quad n_+ n_e \sigma_{fb} f(u)\, u\, du = \frac{4\pi}{h\nu} n_0 \sigma_{bf} \left(1 - e^{-h\nu/kT}\right) B_\nu \, d\nu$$

$$\Rightarrow \frac{\sigma_{bf}}{\sigma_{fb}} = \frac{n_+ n_e}{n_0} \cdot \frac{f(u)\, u\, du}{\frac{4\pi}{h\nu}\left(1 - e^{-h\nu/kT}\right) \cdot B_\nu \, d\nu}$$

$$B_\nu = \frac{2h\nu^3}{c^2} \frac{1}{e^{\frac{h\nu}{kT}} - 1}$$

$$\frac{1}{2} m u^2 + \cancel{\chi} = h\nu \quad \Rightarrow \quad m u\, du = h\, d\nu \quad \Rightarrow \quad \frac{du}{d\nu} = \frac{h}{m u}$$

$$\Rightarrow \frac{\sigma_{bf}}{\sigma_{fb}} = \frac{n_+ n_e}{n_0} \cdot f(u) \cdot \frac{h}{m} \cdot \frac{1}{\frac{4\pi}{\cancel{h\nu}} \cdot \frac{2\cancel{h}\nu^{\cancel{3}2}}{c^2} \cdot \frac{\cancel{\left(e^{h\nu/kT} - 1\right)}}{e^{h\nu/kT}} \cdot \frac{1}{\cancel{e^{\frac{h\nu}{kT}} - 1}}}$$

$$\frac{\sigma_{bf}}{\sigma_{fb}} = \frac{n_+ n_e}{n_0} f(u) \boxed{\frac{h}{m} \frac{e^{h\nu/kT} \cdot c^2}{8\pi \nu^2}}$$

$$\frac{c^2 h}{8\pi m \nu^2}$$

Maxwell:

$$f(u) = 4\pi\left(\frac{m}{2\pi kT}\right)^{3/2} u^2 e^{-\frac{mu^2}{2kT}}$$

Saha:

STAT. weight bare electron, bare proton

$$\frac{n_+ n_e}{n_n} = \left(\frac{2\pi m kT}{h^2}\right)^{3/2} \frac{g_e g_+}{g_n} e^{-\chi/kT}$$

g_n ← level n

$$\Rightarrow \frac{\sigma_{bf}}{\sigma_{fb}} = \left(\frac{2\pi m kT}{h^2}\right)^{3/2} \cdot \frac{g_e g_+}{g_n} e^{-\chi/kT} \cdot \frac{c^2 h}{\cancel{8\pi} m \nu^2} \cdot \cancel{4\pi}\left(\frac{m}{2\pi kT}\right)^{3/2} u^2 e^{-\frac{mu^2}{2kT}} \cdot e^{\frac{h\nu}{kT}}$$

$$e^{\frac{-\chi - \frac{mu^2}{2} + h\nu}{kT}} = 1$$

$$= \frac{g_e g_+}{g_n} \cdot u^2 \cdot \left(\frac{\cancel{2\pi} m \cancel{kT}}{h^2} \cdot \frac{m}{\cancel{2\pi kT}}\right)^{3/2} \cdot \frac{c^2 h}{2m\nu^2}$$

$$\frac{m^{3/2}}{h^{3/2}} \cdot \frac{c^2 \cancel{h}}{2\cancel{m}\nu^2} = \frac{m^2 c^2}{h^2 \nu^2} \cdot \frac{1}{2}$$

$$= \frac{g_e g_+}{g_n} \cdot u^2 \cdot \frac{1}{2} \cdot \frac{m^2 c^2}{h^2 \nu^2}$$

$$\boxed{\frac{\sigma_{bf}}{\sigma_{fb}} = \frac{m^2 c^2 u^2}{h^2 \nu^2} \cdot \frac{g_e g_+}{2 g_n}}$$

$g_e = 2$

$g_+ = 1$

$g_n = 2n^2$

So, in general,

$$\sigma_m^{fb} = \underbrace{\left(\frac{2 g_n}{g_e g_+}\right)}_{= 2n^2} \left(\frac{h\nu}{m_e c u}\right)^2 \sigma_m^{bf}$$

Spont. recombination cross section to level n

u: velocity thermal

Spont. ionization cross section from level n

HII REGIONS

what about absorption of ionizing photons by dust? $\Rightarrow$ number of available photons for ionization decreases by some factor $\longrightarrow$ Spitzer §5.c

$$\tau_s(H) = n_H a_\nu r_s$$ opacity due to H ionization

r_s = radius of dust-free HII region

$\tau_s(H)$ = optical depth out to r_s just shortward of the ionization limit.

Then, using

$$\left.\begin{aligned} N_H &= n_H r_s \\ N_H &= 5.9\times 10^{21}\ E_{B-V} \\ \tau_{d} &= 13\ E_{B-V} \end{aligned}\right\} \text{ we find } \frac{\tau_{sd}}{\tau_{sH}} \approx \frac{1}{3000}$$

τ_{sd}	$y_i = \frac{r_{\text{with dust}}}{r_{\text{wo dust}}}$
0.1	0.98
1.0	0.81
4.0	0.56
20	0.25
40	0.15

fraction of photons absorbed by H rather than dust is y_i^3

See Draine §15.4 for more elaborate discussion

HII Region Diagnostics

Osterbrock §4.2

H emission lines

Recombinations to $n=1$ just produce ionizing photons again, so Ly continuum photons are not observable.

$\Rightarrow$ γ that produce e that recombine to $n=1$ are immediately rejuvenated.

Other possibilities:

a) Go from $n \geq 2$ to $n=1$ (Ly lines)

However, the opacity to Ly photons is very large within a typical HII region (case B for Osterbrock)

$\tau(Ly\alpha) \sim 10^4 \tau(Lyc)$, $\tau(Ly\beta) \sim 10^3$, $\tau(Ly8) \sim 10^2$, $\tau(Ly18) \sim 10$

$\Rightarrow$ These photons are reabsorbed, and each time they have a chance to be converted to Ly + some other series photon (a lower series photon). These Ly photons are resonantly ~~absorbed~~ scattered around until they reach the edge of the HII region, or are absorbed by dust, or the $n=2$ level de-excites via 2-γ emission

b) Go from $n>2$ to $n=2$ (Balmer photons)

These escape. Then $n=2$ $l=0$ $\xrightarrow{1/3}$ 2-γ to $n=1$, $l=0$

$\xrightarrow{2/3}$ Lyα (see previous case)

So every Ly photon ($n \geq 3$) ends up as lower series photons plus either Lyα or two continuum photons that add up to Lyα.

Osterbrock discusses a "Case A", where the nebula is optically thin to Ly photons. It is easy to see that this requires very low densities, making these objects unlikely and difficult to observe.

⇒ Each ionizing photon from * produces one Balmer photon (either Balmer series or continuum), unless there is a lot of dust. This is how the ionizing flux is measured.

Line emissivities are $\propto n_e n_p \cdot f(T)$ since they represent a recombination rate $\left(\sim n_e n_p \cdot \underbrace{f(T)}_{T^{-1/2}}\right)$ to all states times a fraction of the direct recombs + cascades through a given state, times an Einstein A

Osterbrock Tables 4.1–4.2 ⇒ emissivity coeffs.

$4\pi j_0 / n_p n_e$

The Balmer intensity is written in term of an "emission measure" $EM \equiv \int_0^R n_e^2\, ds$

$[EM] = cm^{-6}\, pc$ ⇒

$$I_{line} = \int I_\nu d\nu = h\nu\, \alpha_{mn} \cdot \frac{n_p}{n_e} \cdot 2.46 \times 10^{17}\ EM \quad \text{(Spitzer 3-36)}$$

"effective recombination coeff"

$\alpha_{mn} n_e n_p \triangleq$ Total # of γ emitted per second per cubic cm in transitions from m to n

See Table Spitzer 4.5 + Osterbrock 4.2

HII REGIONS $\alpha_{H\beta} \approx 3.03 \times 10^{-14}\ cm^3/s$ @ 10^4 K

Radio recombination lines (RRLs) are abundant.
Examples are H109α $\Rightarrow$ $\Delta n = 1$, $n = 110 \to 109$
at $\nu = 5008.89$ MHz, H137β $\Rightarrow$ $\Delta n = 2$, $n = 139 \to 137$
$\nu = 5005.0$ MHz, etc. They behave very similarly to optical recomb. lines, but: 1) The gaunt factor is much larger in the radio (recall HIM discussion) and 2) The stimulated emission correction is very important. Some of these lines mase (RRLs masers are not uncommon).
See Spitzer §4.2bc, Osterbrock §4.4

<u>Heavy element emission lines</u> Spitzer §4.1abc
Osterbrock §3.5

Strong features from OII, OIII, and NII
Also lines from SII, NeIII. Important transitions generally associated with orbital angular momentum changes (fine structure). In the conditions in HII regions, transitions are collisionally excited followed by radiative de-excitation. Collisional de-excitation only occurs at very high densities.

Basic general eqn.: detailed balance

$$\underbrace{n_j \left\{ \sum_k \left(\overbrace{n_e \gamma_{jk}}^{\text{collisional}} + \overbrace{B_{jk} J_\nu}^{\text{stimulated depopulation}}\right) + \underbrace{\sum_{k<j} A_{jk}}_{\text{radiative de-exc.}} \right\}}_{\text{losses from level } j} = \underbrace{\sum_k n_k \left(\overbrace{n_e \gamma_{kj}}^{\text{collisions}} + \overbrace{B_{kj} J_\nu}^{\text{stim. rad. population}}\right) + \underbrace{\sum_{k>j} n_k A_{kj}}_{\text{spont. rad. pop. from higher levels}}}_{\text{gains to level } j}$$

Note: Spitzer uses $B_{jk} U_\nu$ to define stimulated emission, where $U_\nu = \frac{4\pi}{c} J_\nu \Rightarrow B_{jk}(\text{shu}) \cdot \frac{c}{4\pi} = B_{jk}(\text{Spitzer})$

Collisional rates come from integrating $\sigma(v)$ over a distribution (Maxwellian) of velocities.

Detailed balance in the collisional-dominated limit means that

$$\underbrace{\gamma_{jk} = \frac{g_k}{g_j} e^{-\frac{E_k - E_j}{kT}}}_{\text{Boltzmann}} \cdot \gamma_{kj} \quad \left(\text{e.g. Spitzer } \begin{matrix}4\text{-}7\\4\text{-}8\end{matrix}\right)$$

↑ stat weights

= collision strength

$$\gamma_{kj} = \frac{h^2 \Omega(j,k)}{g_k (2\pi m_e)^{3/2} (kT)^{1/2}} = \frac{8.63 \times 10^{-6} \, \Omega(j,k)}{g_k T^{1/2}} \ \text{cm}^3 \text{s}^{-1}$$

Spitzer eq. 4-11

See Table 4.1 for values of Ω

Osterbrock: Tables 3.3-3.7 (γ), 3.8-3.10 (A)

Since the radiation field is not very strong, we commonly neglect stim. terms. $\Rightarrow$

$$n_j \left(\sum_{k \neq j} n_e \gamma_{jk} + \sum_{k<j} A_{jk} \right) = \sum_k n_k n_e \gamma_{kj} + \sum_{k>j} n_k A_{kj}$$

These eqs., plus the all-important $\sum_k n_k = n$,

give N indep. eqs. for an N-level system.

k max. is given by the highest level with "significant" population

HII REGIONS

From comparing $\langle n_e \rangle$ to $\langle n_e^2 \rangle$ from emission measure, we get an estimate of the clumping.

How To get Temperature?

Need two widely spaced upper levels, and a closely spaced lower level

eg.: [OIII], [NII]

[OIII]

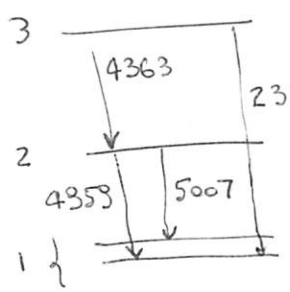

Osterbrock fig. 3.1

By accounting for the various possibilities for the downward path, we can show that:

$$\frac{I_{4363}}{I_{5007} + I_{4959}} \cong 0.12 \exp\left(\frac{-32,900}{T}\right)$$ in the low density limit

(In general, Osterbrock eq. 5.4 $$\frac{I_{4959} + I_{5007}}{I_{4363}} = \frac{7.90 \exp(3.29 \times 10^4 / T)}{1 + 4.5 \times 10^{-4} n_e / T^{1/2}}$$)

$\Rightarrow$ For low density:
1) Temperature from [OIII], [NII]
2) density from [OII], [SII]
3) abundances, from ratios of lines of different elements (Eg., metals vs. Hα)

Schraml & Mezger 1969

more than one component, but the angular resolution of the present survey is not sufficient to allow a reliable decomposition.

The model of a spherical H II region of uniform density has been adopted for the following computations. The following relations were originally derived in Paper I, but are given here in a slightly modified form. Note, however, that the factors $a^{1/2}$ in equations A13 and A14 of Paper I should be in the denominators. At 15 GHz a can deviate from unity by as much as 15 per cent; the factor is therefore retained in the numerical computations. Temperature values have to be substituted in degrees Kelvin (rather than in 10^4 ° K) in the following equations. The diameter of the component (column 11) is computed from

$$2R_s = D\theta_{\rm sph} \,. \tag{3}$$

Distances have been taken from Table 4. The relation $\theta_{\rm sph} = 1.471\, \theta_{\rm G}$ (Paper I) has been used to compute the equivalent angular diameter of a spherical source from the observed HPW of the Gaussian source, $\theta_{\rm G} = \sqrt{(\theta_{\max} \cdot \theta_{\min})}$, which is defined as the geometric mean of major and minor HPW's. The distance z from the galactic plane, given in column 12, has been computed from

$$z = D \sin (b^{\rm II}) \,. \tag{4}$$

In cases where the distance ambiguity has not been resolved (§ IV), the values corresponding to the farther distance of a component are given in brackets.

The electron density (col. 13) is calculated from

$$\left[\frac{N_e}{\rm cm^{-3}}\right] = 98.152 a(\nu,T_e)^{-0.5} \left[\frac{\nu}{\rm GHz}\right]^{0.05} \left[\frac{T_e}{\rm ° K}\right]^{0.175} \left[\frac{S_\nu}{\rm f.u.}\right]^{0.5} \times \left[\frac{D}{\rm kpc}\right]^{-0.5} \left[\frac{\theta_{\rm G}}{\rm min\ arc}\right]^{-1.5} . \tag{5}$$

This relation yields the total number of electrons per cubic centimeter, so the density must be decreased by the factor $1/[1 + N({\rm He}^+)/N({\rm H}^+)]$ for the computation of the total mass of ionized hydrogen (col. 14).

$$(M_{\rm H\,II}/M_\odot) = 9.954 \times 10^{-2} a(\nu,T_e)^{-0.5} \left[\frac{\nu}{\rm GHz}\right]^{0.05} \left[\frac{T_e}{\rm ° K}\right]^{0.175} \left[\frac{S_\nu}{\rm f.u.}\right]^{0.5} \times \left[\frac{D}{\rm kpc}\right]^{2.5} \left[\frac{\theta_{\rm G}}{\rm min\ arc}\right]^{1.5} \left[1 + \frac{N({\rm He}^+)}{N({\rm H}^+)}\right]^{-1} . \tag{6}$$

The emission measure in the center of the source (col. 15) is independent of the distance,

$$\left[\frac{E_c}{\rm pc\ cm^{-6}}\right] = 2R_s N_e^2 = 4122.5 a(\nu,T_e)^{-1} \left[\frac{\nu}{\rm GHz}\right]^{0.1} \left[\frac{T_e}{\rm ° K}\right]^{0.35} \left[\frac{S_\nu}{\rm f.u.}\right] \left[\frac{\theta_{\rm G}}{\rm min\ arc}\right]^{-2} . \tag{7}$$

In addition to these quantities, we have computed the excitation parameter of both individual components and the background (cols. 16 and 17):

$$\left[\frac{u}{\rm pc\ cm^{-2}}\right] = R_S N_e^{2/3} = 4.5526 \left\{ a(\nu,T_e)^{-1} \left[\frac{\nu}{\rm GHz}\right]^{0.1} \left[\frac{T_e}{\rm ° K}\right]^{0.35} \left[\frac{S}{\rm f.u.}\right] \left[\frac{D}{\rm kpc}\right]^{2} \right\}^{1/3} . \tag{8}$$

This is a quantity which can be used to estimate the spectral type of the exciting star (§ VII). All components have been evaluated in the same way for the sake of consistency. Some of the physical parameters of these sources have been derived in more detail elsewhere, and we refer to these cases in the Notes to Table 5.

Table 4.1. Collision Strengths for Excitation by Electrons

Number of p electrons	Ion	Levels Lower	Upper	E_{jk}(eV)	$\Omega(j,k)$	$\Sigma_j A_{kj}(s^{-1})$
1, 5	C II	$^2P_{1/2}$	$^2P_{3/2}$	0.0079	1.33	2.4×10^{-6}
	Ne II	$^2P_{3/2}$	$^2P_{1/2}$	0.097	0.37	8.6×10^{-3}
	Si II	$^2P_{1/2}$	$^2P_{3/2}$	0.036	7.7	2.1×10^{-4}
2	N II	$^3P_0$ —	$^3P_1$	0.0061	0.41	2.1×10^{-6}
		$^3P_0$ —	$^3P_2$	0.0163	0.28	7.5×10^{-6}
		$^3P_1$ —	$^3P_2$	0.0102	1.38	7.5×10^{-6}
		^3P —	$^1D_2$	1.90	2.99	4.0×10^{-3}
		^3P —	$^1S_0$	4.05	0.36	1.1
	O III	$^3P_0$ —	$^3P_1$	0.014	0.39	2.6×10^{-5}
		$^3P_0$ —	$^3P_2$	0.038	0.21	9.8×10^{-5}
		$^3P_1$ —	$^3P_2$	0.024	0.95	9.8×10^{-5}
		^3P —	$^1D_2$	2.51	2.50	2.8×10^{-2}
		^3P —	$^1S_0$	5.35	0.30	1.8
3	O II	$^4S_{3/2}$	$^2D_{5/2}$	3.32	0.88	4.2×10^{-5}
		$^4S_{3/2}$	$^2D_{3/2}$	3.32	0.59	1.8×10^{-4}
		$^2D_{3/2}$	$^2D_{5/2}$	0.0025	1.16	4.2×10^{-5}

Spectroscopic notation:

$$N\,^{2s+1}L_j$$

N = Ppal. quantum number (often omitted)

S = Total spin quantum ~~number~~ number ~~[illegible]~~ (sum of spins of electrons)

2s+1 is the multiplicity

L = Total ~~[illegible]~~ orbital angular momentum quantum #

(noted as S for 0, P for 1, D for 2, F for 3)
"sharp" "principal" "diffuse" "fundamental"

j = actual J (orbital angular momentum) level

For Hydrogen: $1\,^2S_{\frac{1}{2}}$, $2\,^2S_{\frac{1}{2}}$, $2\,^2P_{\frac{3}{2}}$, $2\,^2P_{\frac{1}{2}}$, $3\,^2S_{\frac{1}{2}}$, $3\,^2P_{\frac{3}{2}}$, $3\,^2P_{\frac{1}{2}}$,
$3\,^2D_{\frac{5}{2}}$, $3\,^2D_{\frac{3}{2}}$, etc

:ctrons

$\Sigma_j A_{kj}(s^{-1})$
2.4×10^{-6}
8.6×10^{-3}
2.1×10^{-4}
2.1×10^{-6}
7.5×10^{-6}
7.5×10^{-6}
4.0×10^{-3}
1.1
2.6×10^{-5}
9.8×10^{-5}
9.8×10^{-5}
2.8×10^{-2}
1.8
4.2×10^{-5}
1.8×10^{-4}
4.2×10^{-5}

: orbital and spin
ıcludes g_J separate
1. Usually several
parated slightly in
;hter chemical ele-
a letter S, P, D, or
l so on, for L, the
um (resulting from
e bound electrons).
;pectroscopic term,
ıultiplicity" of that
and so forth. (The
nber for the vector
ins.) An "electron
l l, the total and
ly yields a number
in Table 4.1 corre-
oms listed, and the
ı vector addition of
n a change in the

HII REGIONS

spatial wave functions involved. The subscript number following each letter (S, P, or D) in Table 4.1 is the J value for each particular level.

Energy level diagrams for the ground electron configurations of O II and O III are shown in Fig. 4.1; those for O I and N II are similar to that for O III except that for O I the relative positions of the three fine-structure levels of the ground ^3P term are inverted, with the $J=2$ level ($^3P_2$) the ground state. For excitation of the higher levels of N II and O III, the transitions for all three levels of the ground ^3P term are grouped together to give a total $\Omega(j,k)$ in Table 4.1; each of these three fine-structure levels contributes to $\Omega(j,k)$ in proportion to the statistical weight $2J+1$ for that level.

For each upper level, the sum of the spontaneous radiative transition probabilities, A_{kj}, from that level to all lower levels is given in the last column of Table 4.1 [1,2]. Electric dipole transitions are forbidden for all these transitions, as is generally the case among energy levels of the same electron configuration; hence the radiative transition probabilities given in the last column are all very small.

We consider next the values of γ_{jk} for excitation by H atoms and H_2 molecules. Evidently such collisions are of primary interest in H I regions,

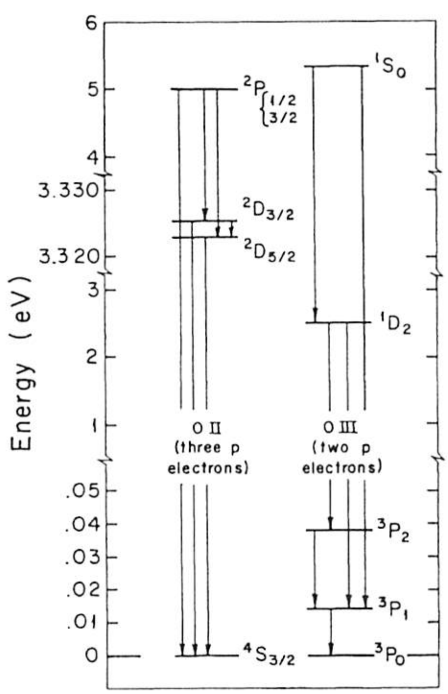

Figure 4.1 Energy level diagram for O II, O III. Each horizontal bar represents an atomic level with an excitation energy shown on the left-hand scale, which changes abruptly to show separation of the fine structure levels in some spectroscopic terms. The forbidden radiative transitions which produce astrophysically important lines are shown by arrows.

SPITZER

$2^2S_{1/2}$ which can only
continuum which rises
the free–free and free–
ogen.

xciting stars and causes
ultraviolet. Dust grains
l some of the Lyman α
d energy in the mid- and
n are quantitatively very
Fig. 7.9.

are emitted by radiative
her levels of these atoms.
hydrogen are shown on
in the infrared hydrogen
rresponding atomic levels
ept for helium (Benjamin
n lines. For the other lines

diagram) for hydrogen. It
the Lyman lines (Case B
ltimately yields a Balmer
a very interesting property
ations, hence the number
of the Balmer continuum
l the *Zanstra method.*
ebula optically thick in the
m it encounters. This atom
trary direction. The Lyman
cattering) until they escape
gion[1]. The $n = 2$ level can
ccur from this level.
ion lines. Since these lines
e population of the levels.

neutral medium, where these
ed by dust. For a study of this
an application to the escape of

HII REGIONS

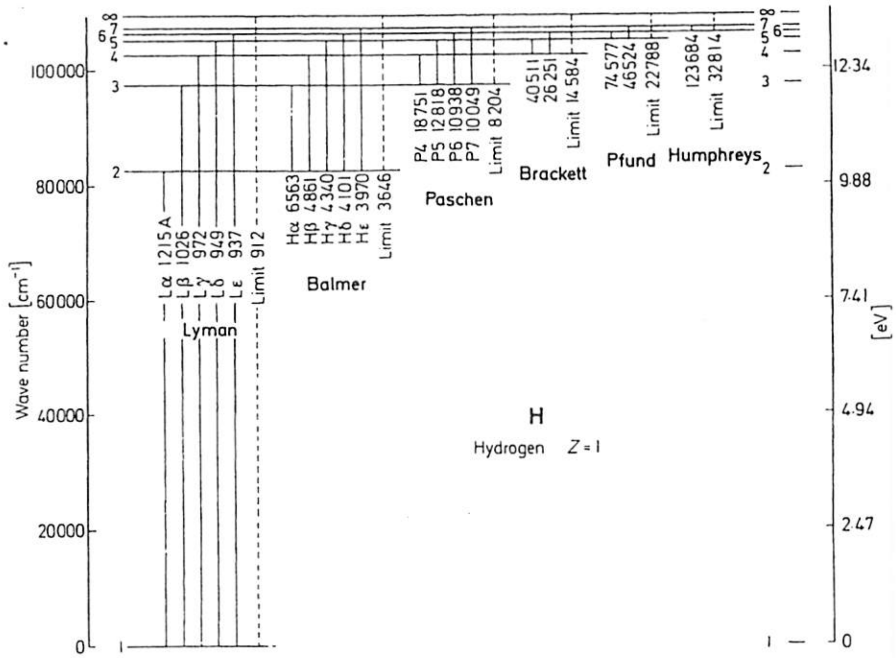

Fig. 5.5. Energy diagram for the hydrogen atom, with the different series designated. The principal quantum number n is indicated to the left of each level. The scale of the ordinate is in wave numbers, $1/\lambda$, and should be multiplied by hc in order to obtain the energies. From Lang [299].

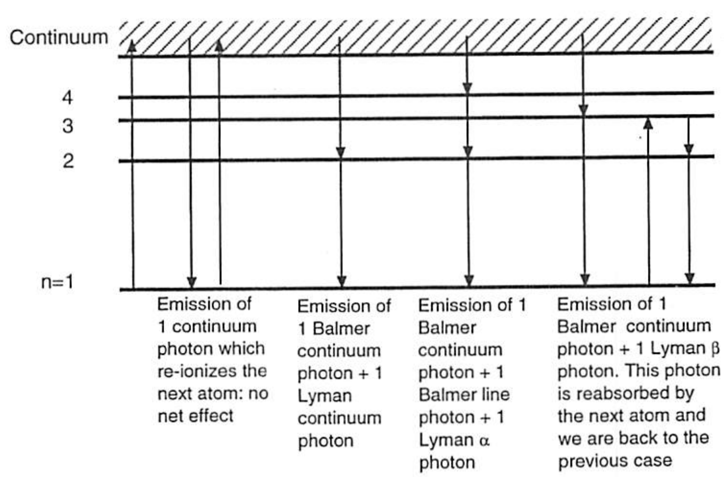

Fig. 5.6. Schematic showing that every recombination of hydrogen in an H II region produces a Balmer photon in case B.

level $2^2S_{1/2}$ which can only
ing a continuum which rises
: than the free–free and free–
hydrogen.

ust

he exciting stars and causes
ı the ultraviolet. Dust grains
; and some of the Lyman α
orbed energy in the mid- and
ssion are quantitatively very
nple Fig. 7.9.

hat are emitted by radiative
higher levels of these atoms.
of hydrogen are shown on
ge in the infrared hydrogen
corresponding atomic levels
xcept for helium (Benjamin
ion lines. For the other lines

n diagram) for hydrogen. It
in the Lyman lines (Case B
ultimately yields a Balmer
a very interesting property
inations, hence the number
r of the Balmer continuum
ed the *Zanstra method*.
nebula optically thick in the
om it encounters. This atom
itrary direction. The Lyman
cattering) until they escape
egion[1]. The $n = 2$ level can
ccur from this level.
tion lines. Since these lines
e population of the levels.

neutral medium, where these
ed by dust. For a study of this
an application to the escape of

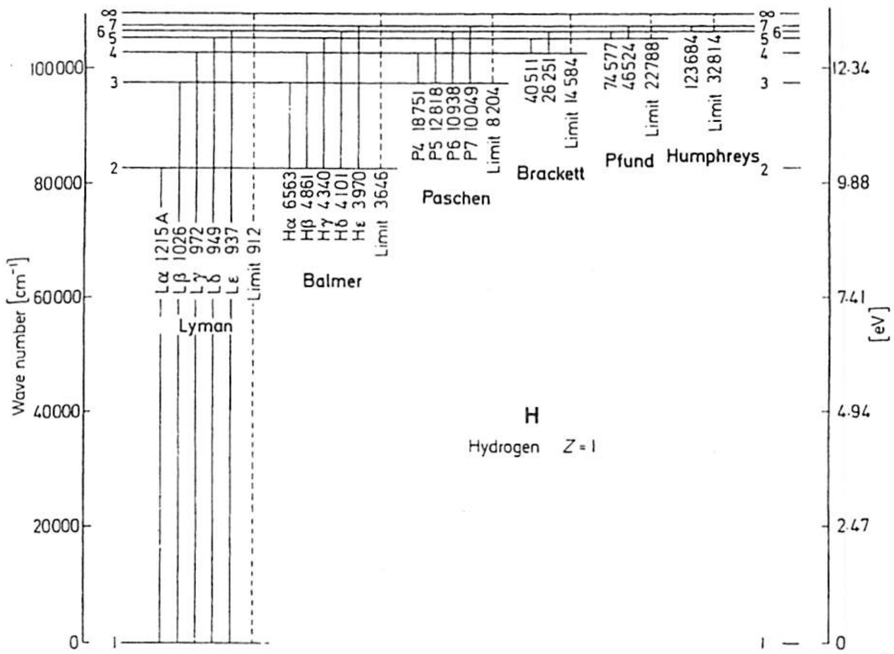

Fig. 5.5. Energy diagram for the hydrogen atom, with the different series designated. The principal quantum number n is indicated to the left of each level. The scale of the ordinate is in wave numbers, $1/\lambda$, and should be multiplied by hc in order to obtain the energies. From Lang [299].

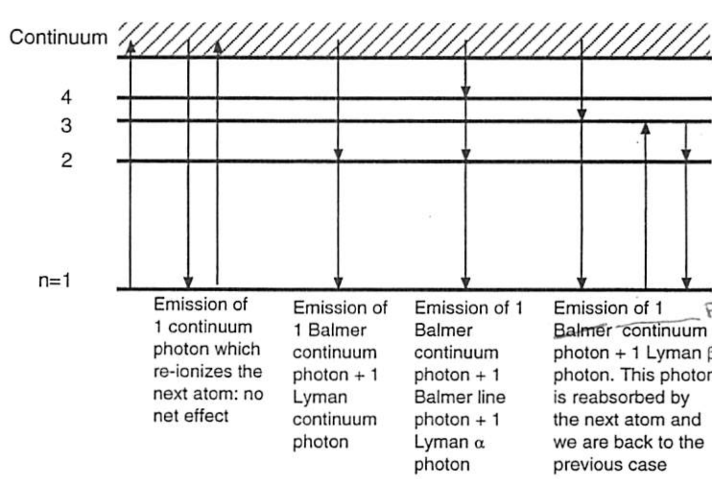

Paschen

Zanstra method
use Balmer info to estimate ionizing flux

Fig. 5.6. Schematic showing that every recombination of hydrogen in an H II region produces a Balmer photon in case B.

LEQUEUX

Table 4.1

$\tau_{Ly} \ll 1$

H I recombination lines (Case A, low-density limit)

	T			
	2,500 K	5,000 K	10,000 K	20,000 K
$4\pi j_{H\beta}/n_e n_p$ (erg cm^3 s^{-1})	2.70×10^{-25}	1.54×10^{-25}	8.30×10^{-26}	4.21×10^{-26}
$\alpha^{eff}_{H\beta}$ (cm^3 s^{-1})	6.61×10^{-14}	3.78×10^{-14}	2.04×10^{-14}	1.03×10^{-14}
Balmer-line intensities relative to Hβ				
$j_{H\alpha}/j_{H\beta}$	3.42	3.10	2.86	2.69
$j_{H\gamma}/j_{H\beta}$	0.439	0.458	0.470	0.485
$j_{H\delta}/j_{H\beta}$	0.237	0.250	0.262	0.271
$j_{H\varepsilon}/j_{H\beta}$	0.143	0.153	0.159	0.167
$j_{H8}/j_{H\beta}$	0.0957	0.102	0.107	0.112
$j_{H9}/j_{H\beta}$	0.0671	0.0717	0.0748	0.0785
$j_{H10}/j_{H\beta}$	0.0488	0.0522	0.0544	0.0571
$j_{H15}/j_{H\beta}$	0.0144	0.0155	0.0161	0.0169
$j_{H20}/j_{H\beta}$	0.0061	0.0065	0.0068	0.0071
Lyman-line intensities relative to Hβ				
$j_{L\alpha}/j_{H\beta}$	33.0	32.5	32.7	34.0
Paschen-line intensities relative to Hβ				
$j_{P\alpha}/j_{H\beta}$	0.684	0.562	0.466	0.394
$j_{P\beta}/j_{H\beta}$	0.267	0.241	0.216	0.196
$j_{P\gamma}/j_{H\beta}$	0.134	0.126	0.118	0.110
$j_{P8}/j_{H\beta}$	0.0508	0.0497	0.0474	0.0452
$j_{P10}/j_{H\beta}$	0.0258	0.0251	0.0239	0.0228
$j_{P15}/j_{H\beta}$	0.00750	0.00721	0.00691	0.00669
$j_{P20}/j_{H\beta}$	0.00310	0.00300	0.00290	0.00280

For hydrogen-like ions of nuclear charge Z, all the transition probabilities $A_{nL,n'L'}$ are proportional to Z^4, so the $P_{nL,n'L'}$, and $C_{nL,n'L'}$ matrices are independent of Z. The recombination coefficients α_{nL} scale as

$$a_{nL}(Z, T) = Z\,\alpha_{nL}(1, T/Z^2);$$

the effective recombination coefficients scale in this same way, and since the energies $h\nu_{nn'}$ scale as

$$\nu_{nn'}(Z) = Z^{2}\nu_{nn'}(1),$$

H II REGIONS

©JTERBROCK

20,000 K

.21 × 10^−26

1.03 × 10^−14

2.69
0.485
0.271
0.167
0.112
0.0785
0.0571
0.0169
0.0071

34.0

0.394
0.196
0.110
0.0452
0.0228
0.00669
0.00280

ı probabilities
re independent

ıce the energies

Table 4.2 $\tau_{L\alpha} >> 1$

H I recombination lines (Case B, low-density limit)

	T			
	2,500 K	5,000 K	10,000 K	20,000 K
$4\pi j_{\mathrm{H}\beta}/n_e n_p$ (erg cm^3 s^{-1})	3.72×10^{-25}	2.20×10^{-25}	1.24×10^{-25}	6.62×10^{-26}
$\alpha^{eff}_{\mathrm{H}\beta}$ (cm^3 s^{-1})	9.07×10^{-14}	5.37×10^{-14}	3.03×10^{-14}	1.62×10^{-14}
	Balmer-line intensities relative to Hβ			
$j_{\mathrm{H}\alpha}/j_{\mathrm{H}\beta}$	3.30	3.05	2.87	2.76
$j_{\mathrm{H}\gamma}/j_{\mathrm{H}\beta}$	0.444	0.451	0.466	0.474
$j_{\mathrm{H}\delta}/j_{\mathrm{H}\beta}$	0.241	0.249	0.256	0.262
$j_{\mathrm{H}\varepsilon}/j_{\mathrm{H}\beta}$	0.147	0.153	0.158	0.162
$j_{\mathrm{H}8}/j_{\mathrm{H}\beta}$	0.0975	0.101	0.105	0.107
$j_{\mathrm{H}9}/j_{\mathrm{H}\beta}$	0.0679	0.0706	0.0730	0.0744
$j_{\mathrm{H}10}/j_{\mathrm{H}\beta}$	0.0491	0.0512	0.0529	0.0538
$j_{\mathrm{H}15}/j_{\mathrm{H}\beta}$	0.0142	0.0149	0.0154	0.0156
$j_{\mathrm{H}20}/j_{\mathrm{H}\beta}$	0.0059	0.0062	0.0064	0.0065
	Paschen-line intensities relative to Hβ			
$j_{P\alpha}/j_{\mathrm{H}\beta}$	0.528	0.427	0.352	0.293
$j_{P\beta}/j_{\mathrm{H}\beta}$	0.210	0.187	0.165	0.146
$j_{P\gamma}/j_{\mathrm{H}\beta}$	0.1060	0.0991	0.0906	0.0820
$j_{P\delta}/j_{\mathrm{H}\beta}$	0.0410	0.0392	0.0368	0.0343
$j_{P10}/j_{\mathrm{H}\beta}$	0.0207	0.0199	0.0185	0.0172
$j_{P15}/j_{\mathrm{H}\beta}$	0.00589	0.00571	0.00530	0.00501
$j_{P20}/j_{\mathrm{H}\beta}$	0.00240	0.00240	0.00220	0.00210
	Brackett-line intensities relative to Hβ			
$j_{Br\alpha}/j_{\mathrm{H}\beta}$	0.1447	0.1091	0.0834	0.0640
$j_{Br\beta}/j_{\mathrm{H}\beta}$	0.0709	0.0578	0.0471	0.0380
$j_{Br\gamma}/j_{\mathrm{H}\beta}$	0.0387	0.0332	0.0281	0.0237
$j_{Br\delta}/j_{\mathrm{H}\beta}$	0.0248	0.0216	0.0186	0.0157
$j_{Br10}/j_{\mathrm{H}\beta}$	0.01193	0.01065	0.00920	0.00796
$j_{Br15}/j_{\mathrm{H}\beta}$	0.00317	0.00295	0.00263	0.00231
$j_{Br20}/j_{\mathrm{H}\beta}$	0.00127	0.00124	0.00109	0.00097

HII REGION

OSTERBROCK

Two-level system

$$n_1 n_e \gamma_{12} = n_2 n_e \gamma_{21} + n_2 A_{21}$$

$$n_2 (n_e \gamma_{21} + A_{21}) = n_1 n_e \gamma_{12}$$ ⟸ same equation

$$n_{TOT} = n_1 + n_2$$ ← conservation

$$\frac{n_2}{n_1} = \frac{n_e \gamma_{12}}{n_e \gamma_{21} + A_{21}} = \frac{\gamma_{21} n_e \frac{g_2}{g_1} e^{-(E_2-E_1)/kT}}{n_e \gamma_{21} + A_{21}}$$

$$= \frac{g_2}{g_1} e^{-\frac{(E_2-E_1)}{kT}} \cdot \underbrace{\left[\frac{1}{1 + A_{21}/n_e \gamma_{21}}\right]}_{= \frac{b_2}{b_1}}$$

$\frac{b_2}{b_1}$ ratio of departure coefficients (Spitzer 4-14)

$\frac{A_{21}}{\gamma_{21}} \triangleq$ critical density "n_{crit}"

$\boxed{\text{Low density:}}$

$\frac{n_{crit}}{n_e} \gg 1 \Rightarrow$ not enough collisions, fast de-excitation
lower level pop in level 2 than in LTE

$$\Rightarrow \frac{n_2}{n_1} \sim \frac{g_2}{g_1} e^{-\frac{\Delta E}{kT}} \cdot \frac{1}{\frac{A_{21}}{\gamma_{21} n_e}} \approx \frac{n_e}{n_{crit}}$$

$\Rightarrow n_2 A_{21} \approx \frac{g_2}{g_1} e^{-\frac{\Delta E}{kT}} n_e \cdot n \gamma_{21} \propto n_e^2$
$(n_1 \approx n)$

$I \propto \int n_2 A_{21} dz \propto \int n_e^2 dz$ (abundance)
$n = X \cdot n_e$

$I \propto \langle n_e^2 \rangle$ "emission measure"

$\boxed{\text{High density:}}$

$\frac{n_{crit}}{n_e} \ll 1 \Rightarrow$ radiation is unimportant, better recover Boltzmann

$\Rightarrow$ occupation follows LTE

HII REGIONS

$$n_2 \approx n_1 \frac{g_2}{g_1} e^{-\Delta E/kT}$$

$$\Rightarrow n_1\left(1+\frac{g_2}{g_1}e^{-\Delta E/kT}\right) = n \quad \Rightarrow n_1 = n\left(1+\frac{g_2}{g_1}e^{-\Delta E/kT}\right)^{-1}$$

$$n_2 = \frac{\frac{g_2}{g_1}e^{-\Delta E/kT}}{1+\frac{g_2}{g_1}e^{-\Delta E/kT}} \cdot n$$

Total line strength $I \propto \int n_2 A_{21} dz \propto \int n\, dz \propto \langle n_e \rangle \cdot X$

$\Rightarrow$ Lines with rapid downward rates (large $\frac{A}{\gamma}$) give $I \propto \langle n^2 \rangle$, lines with slow rates (small $\frac{A}{\gamma}$) give $I \propto \langle n \rangle$

How to find out the density?

Imagine two closely-lying levels for which we can neglect $3 \leftrightarrow 2$

$$\begin{array}{l} \overline{}\ 3 \\ \overline{}\ 2 \\ \\ \overline{}\ 1 \end{array}$$

Then using $\frac{n_3}{n_1}$ divided by $\frac{n_2}{n_1}$:

$$\frac{I_{31}}{I_{21}} = \frac{A_{31}\, n_3\, \nu_{31}}{A_{21}\, n_2\, \nu_{21}} = \frac{\nu_{31}\, g_3\, A_{31}}{\nu_{21}\, g_2\, A_{21}} \left[\frac{1+A_{21}/n_e\gamma_{21}}{1+A_{31}/n_e\gamma_{31}}\right] e^{\underbrace{-(E_3-E_2)/kT}_{\text{small}}}$$

$n_e \to \infty \quad \Rightarrow \quad [\;\;] \to 1$

$n_e \to 0 \quad \Rightarrow \quad [\;\;] \to \frac{\gamma_{31} A_{21}}{\gamma_{21} A_{31}}$

$\Rightarrow$ As long as $n_{crit\,2} \neq n_{crit\,3}$, we have $\frac{I_{31}}{I_{21}} = f(n_e)$

Ex: [OII] $\lambda\lambda$ 3728.8, 3726.2 Å

[SII] $\lambda\lambda$ 6716.4, 6730.8 Å

Osterbrock Fig. 5.8

HII REGIONS

Bremsstrahlung radiation

Spitzer § 3.5
Draine § 10

As for HIM, we have

$$\rho j_\nu = 6.6\times10^{-38} Z^2 m_e m_i T^{-1/2} e^{-h\nu/kT} g_{ff}(\nu) \ \mathrm{erg\ cm^{-3}\ s^{-1}}$$

(Shu 15.28, RL 5.14)

Most of the energy is in the radio, unlike HIM.

$h\nu \sim kT \Rightarrow \lambda = \frac{hc}{kT} \cong 2\,\mu m$ for $T = 8000\,K$

$$g_{ff}(\nu) = \frac{\sqrt{3}}{\pi}\left\{ \ln\frac{(2kT)^{3/2}}{(\pi e^2 Z \nu \sqrt{m_e})} - \frac{5\gamma}{2} \right\} = 9.77\left(1 + 0.130 \log\frac{T^{3/2}}{Z\nu}\right)$$

Spitzer 3-55
Draine 10.5

Absorption opacity is:

$$\rho K_\nu = 3.7\times10^{8}\, T^{-1/2} Z^2 m_e m_i \nu^{-3}\left(1 - e^{-h\nu/kT}\right) g_{ff}\ \mathrm{cm^{-1}}$$

(according to Kirchhoff's law, $j\nu = K_\nu B_\nu(T)$) Spitzer 3-57

In the R-J regime: $\rho K_\nu \cong 0.1731 \left\{ 1 + 0.13 \log\left(\frac{T^{3/2}}{Z\nu}\right)\right\} \frac{Z^2 m_e m_i}{T^{3/2}\nu^2}\ \mathrm{cm^{-1}}$

~~High frequencies~~ $\tau_\nu = \int \rho K_\nu\, ds = 8.24\times10^{-2}\, T^{-1.35}\, \nu^{-2.1} \int m_i m_e\, ds$

$\Rightarrow$ High frequencies, $\tau_\nu \ll 1$, optically thin $I_{obs} = \int \frac{\rho j\nu}{4\pi} ds$

Low frequencies, $\tau_\nu \gg 1$, optically thick $I_{obs} \to B_\nu(T)$

$\Rightarrow$ This can be used to establish the temperature of the nebula (Osterbrock § 5.4). However, there are practical problems having to do with beam size (need to resolve emission to establish brightness)

HII REGIONS

Thermal balance in HII regions

Spitzer 6.1
Osterbrock 3

The equilibrium temperature in HII regions (or in any gas) is determined by the balance between heating and cooling

heating (erg $s^{-1} cm^{-3}$)

$$n \frac{d}{dt}\left(\frac{3}{2}kT\right) - kT \frac{dn}{dt} = \Gamma - \Lambda$$

cooling

change in internal energy of the gas

pdV work

(neglecting conduction)
Spitzer 6-1

Heating processes relevant in HII regions: photoionization from * and diffuse
→ photoelectrons collide w/ plasma and thermalize quickly

Cooling: recombination, line and continuum emission

ions and neutrals (H radiates very weakly)

bremsstrahlung and dust IR

In equilibrium, $\Gamma = \Lambda$

This equilibrium is local, but in the simplest case we can equate gains and losses over the entire nebula and find a "mean" temperature (temperature fluctuations can be important).

More realistically, the Γ term changes locally as the hardness of the field changes when moving away from the star.

Usually we group photoionizations - recomb. in the Γ term, as a "net gain".

1.- Net gain of energy

$$\Gamma_{eff} = \text{erg cm}^{-3}\text{s}^{-1} = n_e n_p \left\{ \alpha^{(1)} \overset{\text{ionization}}{\bar{E}_2} - \sum_j \left\langle \tfrac{1}{2} m_e v^3 \sigma_j \right\rangle \right\}$$

$\bar{E}_2 \triangleq$ mean energy gain per electron from photoionization

$\alpha^{(1)} \triangleq$ recomb. rate to all levels
= ionization " from all levels
= ion. rate from $n=1$

$$\bar{E}_2 = \frac{\int_{\nu_1}^{\infty} h(\nu-\nu_1) S_\nu U_\nu \, d\nu/\nu}{\int_{\nu_1}^{\infty} S_\nu U_\nu \, d\nu/\nu}$$ Spitzer 6-6

ν_1: ionization limit 13.6 eV

S_ν: abs. coeff Spitzer 5-6

$$S_\nu = \frac{7.91 \times 10^{-18}}{Z^2} \left(\frac{\nu_1}{\nu}\right)^3 g_\nu \text{ cm}^2$$

for hydrogenic atoms

$\sigma_j \triangleq$ recomb. cross section to level j

near $*$, we assume stellar BB for radiation field, of color temp. T_c $\Rightarrow \bar{E}_2 = \psi_0 k T_c$ $\quad \psi_0 \approx 1$

Table 6.1 Spitzer

Using recomb. cross-section discussed before (Spitzer 5-12 to 5-14), the second term is

$$\frac{1}{2} m_e \cdot \frac{2 \overset{\text{recapture constant}}{A_r}}{\sqrt{\pi}} \left(\frac{2kT}{m_e}\right)^{3/2} \beta \chi_k(\beta)$$

$k=1 \rightarrow$ recomb. to all levels

$k=2 \rightarrow$ recomb to $n>1$

$\beta \triangleq \frac{h\nu_1}{kT}$

$A_r = 2.105 \times 10^{-22}$ cm^2 Spitz 5-10

χ_k = Table 6.2

Near the star:

$$\Gamma^{local}_{eff} = \frac{2.07 \times 10^{-11} n_e n_p}{T^{1/2}} \left\{ \overset{\text{Table 6.1, } \bar{E}_2 = \psi_0 kT_c}{\bar{E}_2} \underset{\text{Spitzer Table 5.2}}{\phi_1(\beta)} - kT \underset{\text{Spitzer Table 6.2}}{\chi_1(\beta)} \right\} \text{ erg cm}^{-3}\text{s}^{-1}$$

Spitzer 6-9

Over the entire HII region, the balance is slightly different: 1) need to include diffuse contribution, 2) recomb. to $n=1$ don't count for cooling.

$$\langle E_2 \rangle = \frac{\int h(\nu-\nu_1)\, U_{\nu,*}\, d\nu/\nu}{\int U_{\nu,*}\, d\nu/\nu}$$

The average mean energy over the entire region

Total kinetic energy imparted to e^-, divided by total rate @ which ionizing photons leave the star

This is not local. Every UV photon ends up as a photoionization somewhere, we need not consider S_ν.

$\langle \bar{E}_2 \rangle = \langle \psi \rangle kT_e$ Tabulated in 6.1 $(\simeq 1)$

Losses: consider only recombs. to $n \geq 2$, since Lyα photons are reabsorbed

$$\Rightarrow \Gamma^{global} = \frac{2.07\times10^{-11}\, n_e n_p}{T^{1/2}} \left\{ \bar{E}_2 \phi_2(\beta) - kT\, \chi_2(\beta) \right\} \text{ erg cm}^{-3}\text{s}^{-1}$$

Cooling

→ forbidden line emission

→ free-free radiation

Since typical es have $kT \sim 1$eV, those are the most important transitions to consider as they are collisionally excited (OII, OIII, NII, etc)

$\Lambda \propto n_e n_p \cdot f(T)$

↑ collisions, $n_i \propto n_p$ approx.

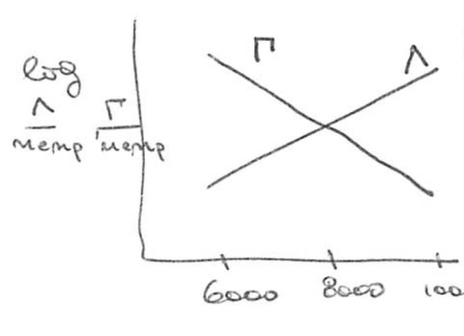

Osterbrock fig. 3.2

Temperature is regulated!

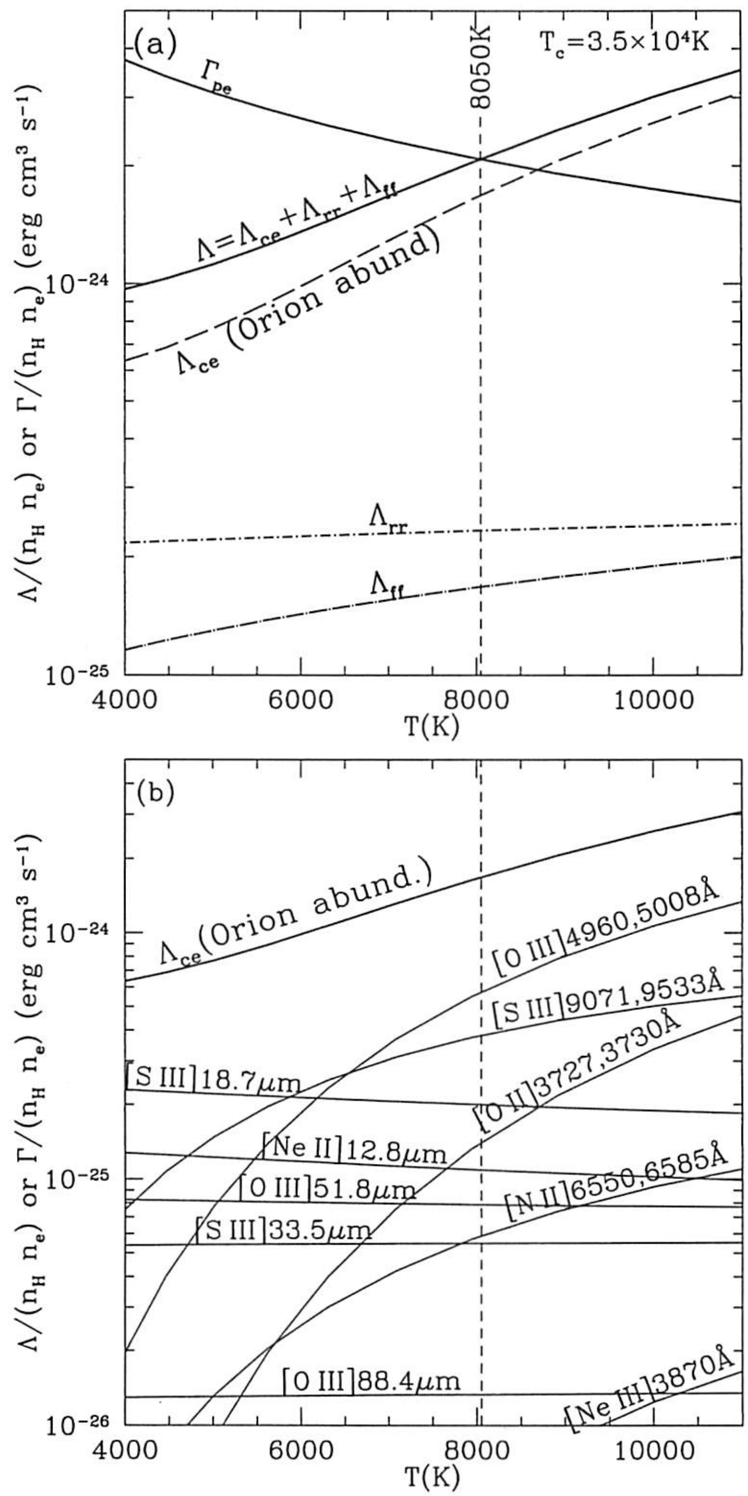

Figure 27.1 (a) Photoelectric heating function Γ_{pe} and radiative cooling function Λ as functions of gas temperature T in an H II region with Orion-like abundances and density $n_{\rm H} = 4000\,{\rm cm}^{-3}$. Heating and cooling balance at $T \approx 8050\,{\rm K}$. (b) Contributions of individual lines to Λ_{ce}.

27.3.3 Collisionally Excited Line Radiation

In an H II region, most of the hydrogen will be ionized. Even if some He or He$^+$ is present, the energy of the first excited state is so far above the ground state that the rate for collisional excitation is negligible. However, if heavy elements such as

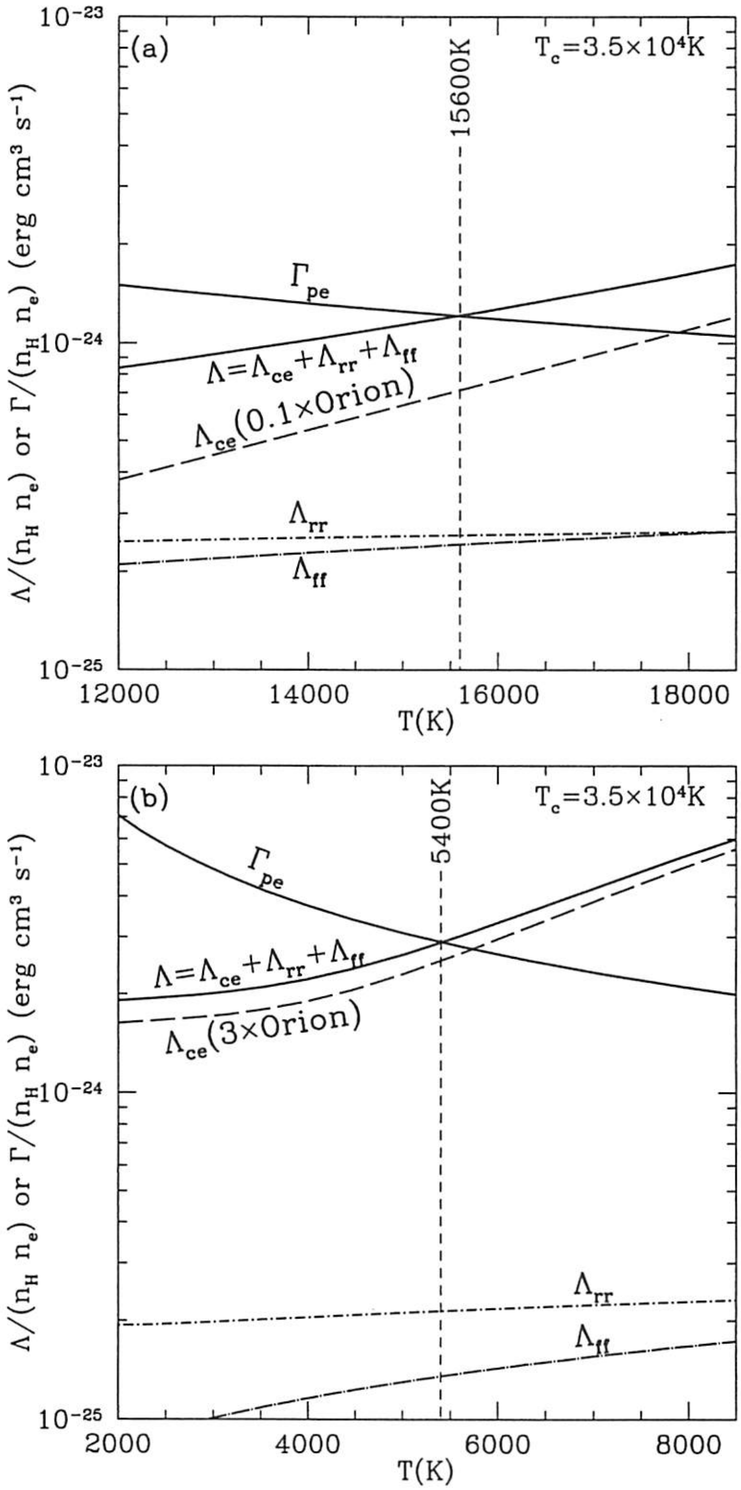

Figure 27.2 (a) Photoelectric heating function Γ_{pe} and radiative cooling function Λ as functions of temperature T in an H II region with abundances that are (a) only 10%, or (b) enhanced by a factor of 3 relative to the Orion Nebula. A density $n_{\rm H} = 4000\,{\rm cm}^{-3}$ is assumed. Thermal equilibrium occurs for $T \approx 15600\,$K and $\sim 5400\,$K for the two cases.

heavy-element abundances by a factor of 3, as might be appropriate in the central regions of a mature spiral galaxy, the H II region temperature drops to just $\sim 5400\,$K.

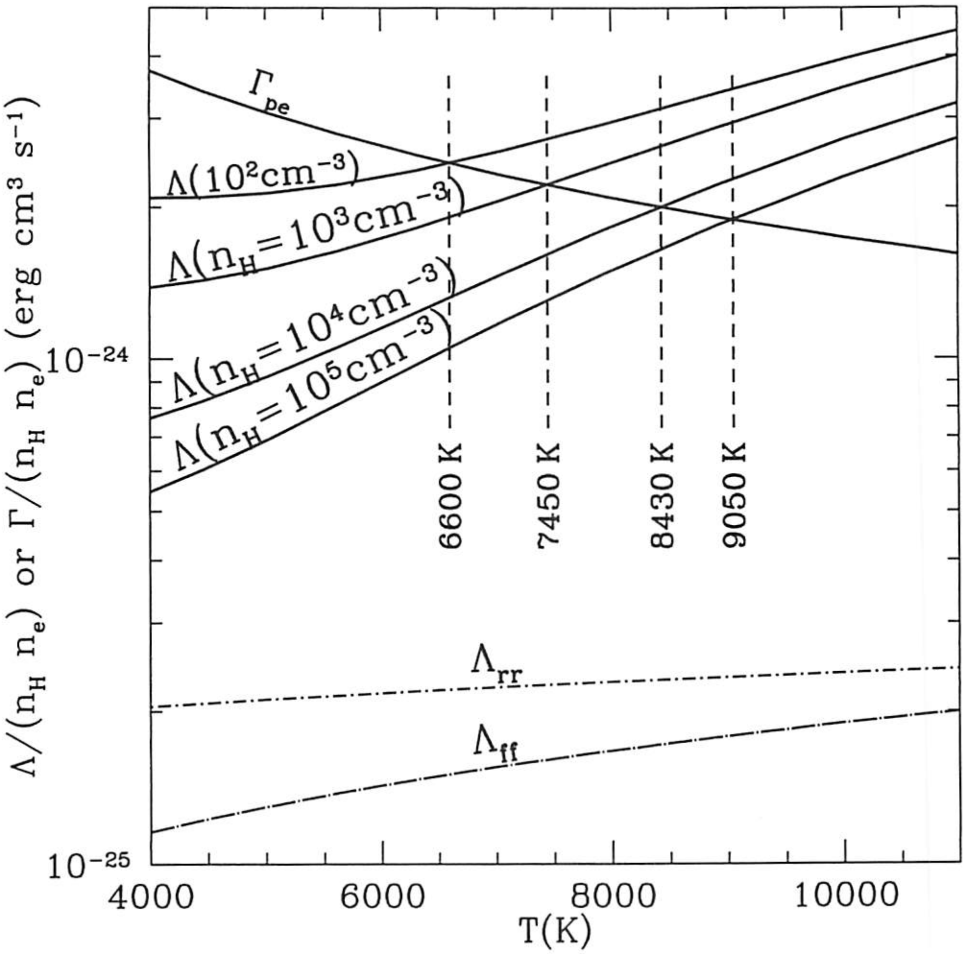

Figure 27.3 Cooling function $\Lambda(T)$ for different densities n_{H}. The gas is assumed to have Orion-like abundances and ionization conditions. As the gas density is varied from 10^2 cm^{-3} to 10^5 cm^{-3}, the equilibrium temperature varies from 6600 K to 9050 K, because of collisional deexcitation of excited states.

For a given ionizing star and gaseous abundances, the H II region temperature will also be sensitive to the gas density. When the density exceeds the critical density of some of the cooling levels, the cooling will be suppressed, and the equilibrium temperature will rise. Figure 27.3 shows how, at fixed Orion Nebula-like abundances and ionization balance, the cooling function $\Lambda(T)/n_{\mathrm{H}}n_e$ responds to changes in the density. As the density is increased from $n_{\mathrm{H}} = 10^2\,\mathrm{cm}^{-3}$ to $n_{\mathrm{H}} = 10^5\,\mathrm{cm}^{-3}$, the thermal equilibrium temperature shifts from 6600 K to 9050 K.

27.5 Emission Spectrum of an H II Region

When the gas is near thermal equilibrium, the principal cooling lines are shown in Fig. 27.1(b), and listed in Table 27.2.

The optical spectrum of an H II region is dominated by the major hydrogen recombination lines (H α 6565 Å, H β 4863 Å, H γ 4342 Å), and collisionally excited